ELSEVIER

0966-9795(95)00023-2

Intermetallics 4 (1996) 85–90

0966-9795/96/$15.00

Microstructure and mechanical properties of Ni–Al and Ni–Al–B alloys produced by rapid solidification technique

M. S. F. Lima* & P. I. Ferreira

Instituto de Pesquisas Energéticas e Nucleares, 05508-900, São Paulo, SP. Brazil

(Received 29 December 1993; accepted 10 March 1995)

Rapidly solidified Ni–Al intermetallic ribbons were produced by chill-block melt spinning in the composition range 68–90 at.% Ni with and without small additions of boron (200, 2000, 4000 wt.ppm). The microstructures of the ribbons were investigated by X-ray diffraction and transmission electron microscopy. The results can be explained based on Norbaskhsh and Chen's metastable phase diagram, in the Ni_3Al region. The microstructure in the hypoeutectic compositions shows an absence of anti-phase domain boundaries. The microstructure in the hypereutectic compositions shows a bimodal distribution of anti-phase domains. Composition effects in yield strength and ductility were investigated by uniaxial tensile tests at room temperature. It was noticed that the yield strength increases when boron content increases from 200 up to 2000 wt.ppm B. It was observed that the boron level at 200 and 2000 wt.ppm did not influence the ductility. Ribbons with 4000 wt.ppm B are brittle. The mechanical properties can be explained in terms of the observed microstructures.

Keywords: A. nickel aluminides, based on Ni_3Al, B. ductility, B. yield stress, D. defects: antiphase domains.

1 INTRODUCTION

In recent years, ordered intermetallic alloys have appeared as structural materials for several applications.[1,2] The Ni–Al intermetallic alloys, NiAl and Ni_3Al, have raised interest because of their attractive high temperature properties[3]. Their low density, high oxidation resistance and unusual yield strength dependence on temperature have led some researchers to develop nickel aluminides alloys for special applications.[4]

The main obstacle in the use of nickel aluminides, like some other intermetallic alloys, is related to their low ductility in a polycrystalline state at room temperature. This low ductility has been attributed to the inherent weakness of grain boundaries.[5] An acute increase in ductility was observed when a small amount of boron (less than 1 at.%) is added to Ni_3Al.[6,7]

*Present address: Departamento de Engenharia Metalúrgica e de Materiais, Escola Politécnica da USP, 05508-900, São Paulo-SP, Brazil.

However, the microstructural features in rapidly solidified nickel aluminide alloys have some conflicting results in literature:

Baker *et al.*,[8,9] have investigated the microstructure of rapidly solidified Ni_3Al powders and they verified the presence of a martensitic phase composed of β'–NiAl with Ll_0 structure in an ordered matrix with Ll_2–Ni_3Al structure.

Horton and Liu[10] have studied hyperstoichiometric Ni_3Al alloys (76 at.% Ni) produced by rapid solidification at some cooling rates. Their structures were composed basically of a bimodal distribution of anti-phase domains (APD) in Ni_3Al grains.

Huang *et al.*[11,12] have analyzed the microstructure of stoichiometric Ni_3Al alloys obtained by melt spinning. They verified the presence of equiaxial grains with a $L1_3$ structure and a second phase, rich in aluminum, which contained twinned martensite.

Cahn *et al.*[13,14] have produced several Ni_3Al ribbons in the range 75–78 at.% Ni. They observed a bimodal distribution of APD in alloys containing 77

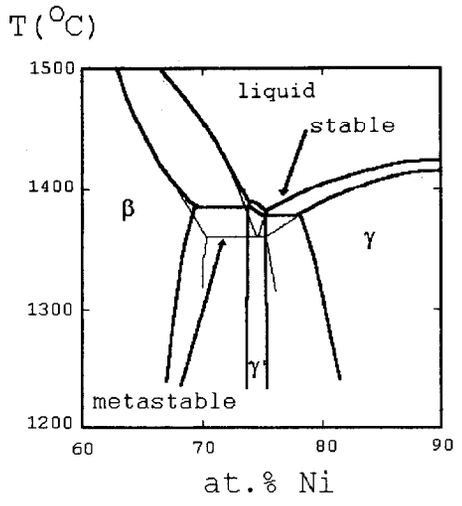

Fig. 1. Metastable phase diagram for Ni–Al alloys, as proposed by Nourbakhsh and Chen.[16] On the stable diagram (thick line), one can be note the β'-NiAl, γ'-Ni_3Al and γ-Ni phases and the peritectic reactions which originates Ni_3Al intermetallic. On the metastable diagram (thin line), the reaction turns up a eutectic β/γ with eutectic composition near 73 at.% Ni.

and 78 at.% Ni, in accordance with Horton and Liu.[10] However, for the alloys containing 74 and 75 at.% Ni, they were not able to observe such APD structures.

Nourbakhsh and Chen[15] investigated Ni–Al alloys containing nickel in the range 61·3–76·0 at.% Ni, produced by the hammer and anvil technique. They proposed a metastable phase diagram, as can be seen in Fig 1. It was noticed that a change in solidification behavior of Ni_3Al from a peritectic to a eutectic reaction occurs near 73 at.% Ni. The eutectic is composed from the B2-martensitic phase and γ–Ni disordered phase; these phases react forming γ'–Ni_3Al. These authors studied mechanical properties of the alloys above through bend ductility tests at room temperature.

However, other authors have produced few contributions on the knowledge of mechanical properties of the rapidly solidified Ni–Al–B alloys in the composition range of the β'-γ phases.

The aims of this work are to understand the observed microstructure in the composition range of 68–90 at.% Ni, correlating this microstructure to the mechanical properties of as-cast ribbons at room temperature.

2 EXPERIMENTAL

Nickel, aluminum and boron (in NiB form), with commercial purity, were used to produce small 8–10 g cast samples that were remelted in melt spinner crucible and then ejected into a rotating steel wheel producing rapidly solidified ribbons. The ribbons had 3 mm diameter, 200 ± 20 μm thickness and several metres length. The calculated cooling rate was approximately 3×10^5 K/s.[16]

Table 1. Composition of the alloys

Composition of alloys
68·0 at.% Ni–0·0 at.% B
71·9 at.% Ni–0·2 at.% B
72·8 at.% Ni–0·02 at.% B
73·0 at.% Ni–0·02 at.% B
74·5 at.% Ni–0·2 at.% B
75·6 at.% Ni–0·02 at.% B
75·9 at.% Ni–0·4 at.% B
76·1 at.% Ni–0·2 at.% B
76·5 at.% Ni–0·2 at.% B
76·8 at.% Ni–0·4 at.% B
78·6 at.% Ni–0·0 at.% B
78·8 at.% Ni–0·2 at.% B
83·6 at.% Ni–0·02 at.% B
84·0 at.% Ni–0·0 at.% B
88·9 at.% Ni–0·02 at.% B

Suitable specimens for TEM analysis were prepared by double jet polishing in a solution of 10% perchloric acid in methanol. The phases were determined by X-ray diffraction using CuKα radiation. Tensile tests to measure 0.2% offset yield strength and plastic deformation (ductility) of as quenched ribbons (l = 50 mm) were carried out at a strain rate of $1·7 \times 10^{-4} s^{-1}$. The values of yield strength and ductility were obtained through six tests with a fixed composition.

The compositions of the ribbons were measured using plasma spectrometry (ICP/AES) and wavelength differential scanning microscopy, as can be seen in Table 1.

3. RESULTS AND DISCUSSION

3.1 Phases and Microstructure

Figure 2 shows the martensite lamellae and the electron diffraction pattern for alloys containing 68·0 at.% Ni. The lamellae are about 0·3 μm. The structural analysis by X-ray and transmission electron diffraction identified a $L1_0$-NiAl phase with a = 3·70 Å and c/a relation around 0·9.

The observed martensitic microstructure agrees with Enami and Nenno[17] and Nourbakhsh and Chen.[15] This microstructure is related to the martensitic transformation of a previous high temperature B2-NiAl phase during cooling in solid state.

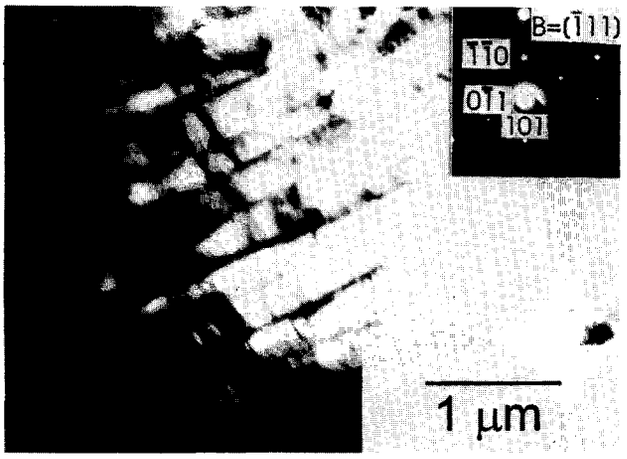

Fig. 2. Transmission electron micrograph (Bright Field—BF) and electron diffraction (**B** = [001] of 68 at.% Ni alloy martensite. The average width of the martensitic plates is about 0·3 μm and are twinned due to mechanical deformation during preparation. Electron diffraction pattern (accompanying XRD analysis) gives a lattice parameter a = 3.70 Å and c/a relation near 0·9.

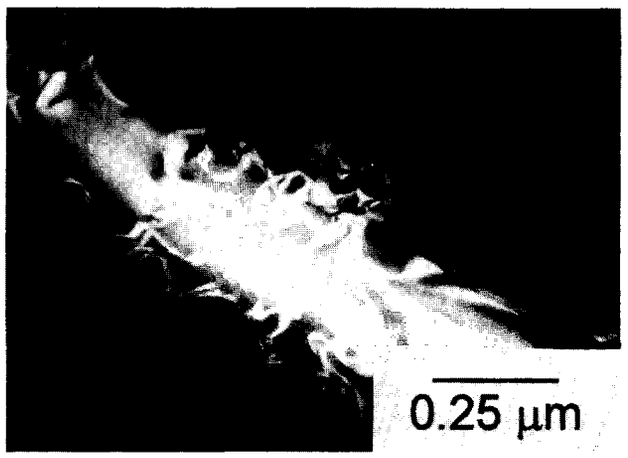

Fig. 4. Transmission electron micrography (Dark Field-DF, **B** = [001]) showing grain boundary region with fines APDB in alloy containing 72·8 at.% Ni.

The characteristic aspect of alloys containing nickel in the range 71·9–73·0 at.% Ni was the partial absence of anti-phase domain boundaries (APDB). There are not any noticeable anti-phase domains (APD) in the core region of the grains, as can be seen in Fig. 3. However, one can notice a thin region near the grain boundaries with small APD (Fig. 4). Furthermore, a fine low volume concentration NiAl-martensite phase was observed in the γ' grains during transmission electron microscopy, as can be seen in Fig. 5. These observations agree with those of the alloys in the range 69·2–73·8 at.% Ni in the Nourbaksh and Chen work[15]. Electron and X-ray diffraction analysis showed only $L1_2$-Ni_3Al structure; the martensitic crystals were very small and in low volume concentration.

The microstructure of the alloys containing 71·9–73·0 at.% Ni can be explained in terms of the metastable phase diagram, as can be seen in Fig. 1.[15] The eutectic composition is situated near 73 at.% Ni. At the beginning of solidification, β crystals grow and the liquid increases its own Ni content. When peritectic temperature is reached, the β-NiAl phase cannot react with the liquid because of the high cooling rate. Thus, the γ'-Ni_3Al phase can be formed directly from saturated liquid.

If the segregation of Ni atoms from the solidification interface reaches a critical value, the formation of the Ni-enriched γ-phase is possible at the completion of solidification. These regions

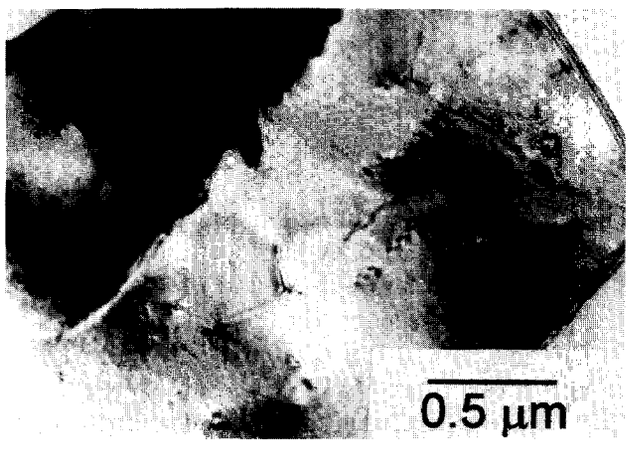

Fig. 3. Transmission electron micrograph (BF) showing ordered Ni_3Al grain with absence of APDB in alloy containing 73·0 at.% Ni. The micrography shows some super-dislocations.

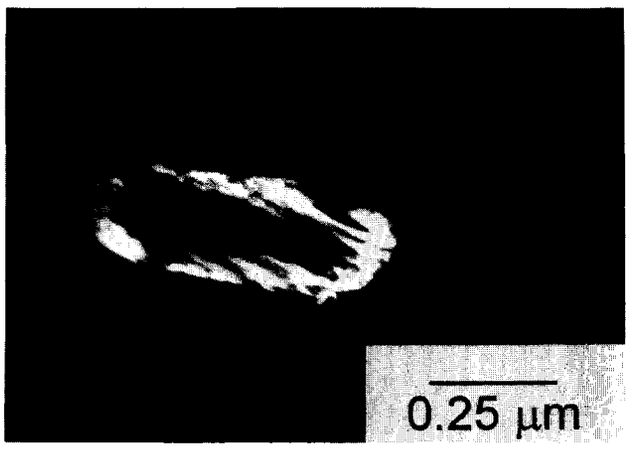

Fig. 5. Transmission electron micrograph (DF) of the martensite phase in the alloy containing 71·9 at.% Ni. These precipitates were observed in the γ' grains which also had martensite plates of about 0·2 μm width.

undergo a disorder–order transformation in solid state generating small domains.[13,14] This behavior can be observed in regions with fine APD near grain boundaries (Fig. 4).

As can be seen in the metastable phase diagram (Fig. 1), the maximum solubility of Al in the γ phase increases up to 24 at.%. In addition, the maximum content of Ni in the β phase is also increased and the β phase (B2 structure) is transformed to the β' martensitic phase (Ll_0 structure) by solid state reaction. Furthermore, the high aluminum content of the γ phase provides the driving force for transformation in the γ'-Ni_3Al ordered structure.

The microstrutures of the alloys with compositions between 74·5 and 78·8 at.% Ni change with regard to the others listed above. The grains are composed of a bimodal distribution of anti-phase domains: coarse near grain boundaries and fine in the core regions of the grains (Fig. 6). Small martensite precipitates were already occasionally found near grain boundaries. XRD analysis showed a Ll_2-Ni_3Al structure.

For the hypereutectic alloys, 74·5 – 78·8 at.% Ni, the γ-Ni(Al) disordered phase solidifies first. The high Al content γ phase cannot assume extensive order during solidification because of the high nickel content, resulting in small domains during solid state cooling.[13,14] The final γ phase, which solidifies at the completion of the solidification process is rich in Al, and this one solidifies directly into the γ' phase. This behavior explains the bimodal distribution of anti-phase boundaries (Fig. 6). The APDB density grows with the nickel content up to 78·8 at.% due to the sequential ordering process in hypereutectic alloys.

Fig. 6. Transmission electron micrograph for the alloy containing 74·5 at.% Ni, showing bimodal distribution of anti-phase domains: coarse near grain boundaries and fine in the core regions of the grains.

Fig. 7. Transmission electron micrograph showing dendrite arms in the alloy contain 76·8 at.% Ni. Indeed, a bimodal distribution of APDB is noticed: fines (central region) and coarse (outer region), as consequence of the solute segregation behavior (see text).

Indeed, the solidification of this region is dendritic. The separation of small domains regions is related to dendrite arm spacing (Fig. 7).

Alloys with composition between 83·6 and 88·9 at.% Ni contain only disordered γ phase. No difference was found in the microstructure for alloys containing 0, 200 and 2000 wt.ppm boron. However, an intergranular boride phase, with the $M_{23}B_6$ structure, was detected in the 4000 wt.ppm B alloy during TEM analysis.

3.2 Mechanical Properties

The mechanical properties of as-cast ribbons at room temperature are summarized in Figs. 8 and 9. Because the alloys with 0 and 4000 wt.ppm boron are brittle, only the 200 and 2000 wt.ppm boron curves were plotted.

As the Ni content increases up to about 76 at.% Ni, an increase in the yield strength was observed. Thereafter, the yield strength decreased in both 200 and 2000 wt.ppm B alloys. This behavior has also been reported by Liu *et al.*[18] for alloys containing between 75–76 at.% Ni and 500 wt.ppm B. The first side of the curve, i.e. between 73–76 at.% Ni, can be explained by the decrease in the volume fraction of the β' phase and the partial disorder, as can be seen by the increasing number of APDB defects. On the other hand, for alloys containing more than 76 at.% Ni, observing the γ-Ni(Al) phase decreases the yield strength because Ni is very ductile. The shifting of strength peak from the eutectic composition, near 73 at.% Ni, to 76 at.% Ni indicates that the nickel enrichment in

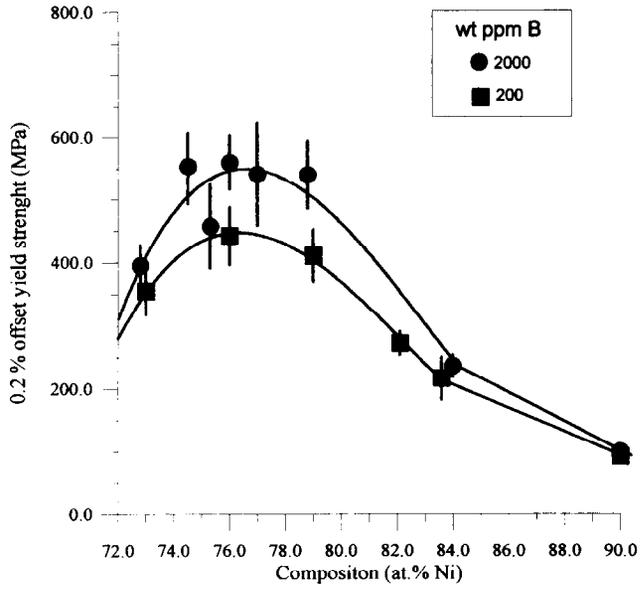

Fig. 8. Mechanical properties: yield strength versus composition plot for ductile Ni–Al–B alloys, with 200 (■) and 2000 (●) wt.ppm B. The maximum strength is viewed near 76 at.% Ni for both boron dopation levels.

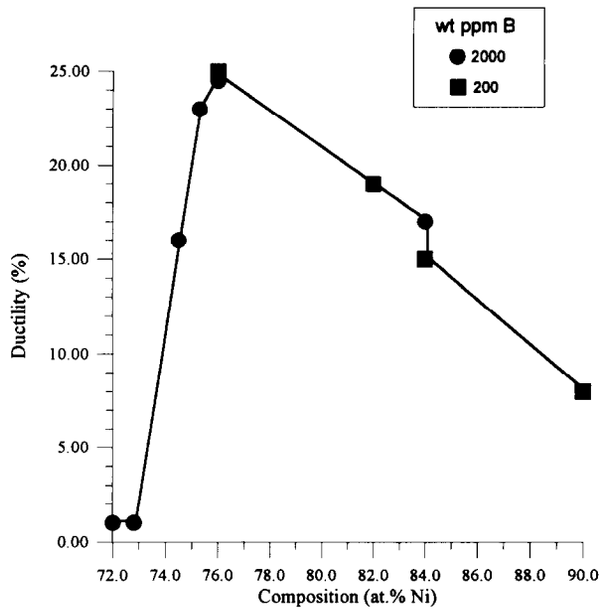

Fig. 9. Mechanical properties: ductility (plastic deformation) versus composition for Ni–Al–B alloys, with 200 (■) and 2000 (●) wt.ppm B. Seemingly, there is no effect of the boron dopation level, 200 and 2000 wt.ppm, on the ductility. The maximum ductility is reached at about 76 at.% Ni.

the grain boundaries region has important effects on the strength.

When the boron content in alloys with Ni content less than 80 at.% increases from 200 to 2000 wt.ppm, the yield strength increases up to 22%. Fig. 8 shows solid solution hardening of boron atoms in the Ni_3Al phase. Seemingly, boron does not promote the solid solution hardening in the γ-Ni(Al) phase. Thus, when the content of the γ-Ni(Al) phase increases, the difference between the 200 and 2000 wt.ppm B curves decreases. This behavior has also been noticed by Huang *et al.*[11] and Liu *et al.*[18]

Figure 9 shows the ductility curve for as-cast ribbons. It can be seen that ductility increases dramatically when Ni content increases up to 76%. The maximum ductility, 25%, can be noticed at 76 at.% Ni. A smooth descending curve can be observed for compositions above 76 at.% Ni. This behavior can be explained in terms of the increase in the γ-Ni(Al) content, because this phase is very ductile at room temperature.

The maximum value obtained for both ductility and tensile strength are positioned at the same composition, 76 at.% Ni. Two different mechanisms explain this observed behavior, because commonly ductility decreases as the strength increases. On the one hand, ductility increases with Ni content up to 76 at.% Ni because boron increases the Ni interatomic cohesion in the γ' phase. On the other hand, boron produces high strengthening effects due to interstitial solid solution hardening.

The ductility test showed an irregular curve on the Ni-rich side. The ductility decreases whilst Ni content increases from 76 at.% up to 84 at.% Ni. Nevertheless the expected procedure is the increase in Ni content due to the softness of Ni. The effect of ordered domains embedded in a disordered matrix might explain this. A general study on the effect of composition on the long range order parameter and its influence in the ductility will be published elsewhere.[19]

The different doping degrees, 200 and 2000 wt.ppm B, do not affect ductility. Alloys without boron and with 4000 wt.ppm are brittle.

4 CONCLUSIONS

Regarding the observed microstructures and mechanical properties of Ni–Al and Ni–Al–B alloys produced by melt spinning, the following is concluded:

(a) Alloys containing 68 at.% Ni had thin martensitic lamellae with $L1_0$ structure.
(b) Alloys containing nickel in the range 71·9–73.0% presented a partial absence of APDB in γ' grains. We also found that fine precipitates were in the β' phase.
(c) Alloys containing nickel in the range 74·5–78·8.% had a bimodal distribution of ordered domains: fine in the central region

and coarse in the surroundings of the γ' grains. This observation can be explained based on the metastable phase diagram, as proposed by Nourbakhsh and Chen.[15] In addition, two mechanisms are proposed for the ordering process for the formation of the γ' phase: direct for hypoeutectic alloys and sequential for hypereutectic alloys.

(d) Alloys containing nickel in the range 83·6–88·9% only have grains of the disordered phase γ.

(e) Both yield strength and ductility show a maximum value near 76 at.% Ni. The effect of boron on the strength and ductility is large. The maximum ductility for both 200 and 2000 wt.ppm B alloys is 25%. The yield strength increases up to 22% for ductile alloys containing 2000 wt.ppm of B. This shows the hardening effect of boron in Ni_3Al alloys. Alloys with 4000 wt.ppm of boron are brittle because of the boride segregation at grain boundaries.

ACKNOWLEDGEMENTS

The authors wish to thank J. C. Dutra for his contributions to the preparation of manuscript. This work was supported in part by CNP_q (Brazilian Government).

REFERENCES

1. Yang, J. M., Kao, W. H. & Liu, C. T., *Metall. Trans.*, **20A** (1989) 2459.
2. Jones, R. H., Henager Jr., C. H., Trzaskoma, P. P., Stoloff, N. S., Moffat, T. S., & Lichter, B. D., *J. Metals,* December (1988) 18.
3. Liu, C. T. & Stiegler, J.O., *Science,* **226** (1984) 636.
4. Larsen, J. M. & Love, D. B., *Industrial Heating,* April (1991) 38.
5. Taub, A. L., Huang, S. C., & Chang, K. M., *Metall. Trans,* **15A** (1984) 199.
6. Aoki, K. & Izumi, O., *J. Mat. Sci.*, **14** (1979) 1800.
7. Aoki, K. & Izumi, O., *J. Japan Inst. Met.*, **43** (1979) 1190.
8. Baker, I., Ichishita, F. S., Surprenant, V. A. & Schulson, E. M., *Metallography,* **17** (1984) 299.
9. Baker, I., Horton, J. A. & Schulson, E. M., *Metallography,* **19** (1986) 63.
10. Horton, J. A. & Liu, C. T., *Acta Metall,* **33** (1985) 2191.
11. Huang, S. C., Chang, K.-M. & Taub, A. L., *Rapidly Solidified Materials*, eds P. W. Lee & R. S. Carbonara, American Society of Metals, Ohio, USA, 1986, p. 255.
12. Taub, A. I., Chang, K.-M. Huang, S. C., *Rapidly Solidified Materials* eds P. W. Lee & R. S. Carbonara, American Society of Metals, Ohio, USA, 1986, p. 97.
13. Cahn, R. W., Siemers, P. A., Geiger, J. E. & Bardhan, P., *Acta Metall,* **35** (1987) 2737.
14. Cahn, R. W., Siemers, P. A. & Hall, E. L., *Acta Metall.*, **35**, (1987) 2753.
15. Nourbakhsh, S. & Chen, P., *Acta Metall.*, **6** (1989) 1573.
16. Lima, M. S. F., Produção e Caracterização Microestrutural e Mecânica de Aluminetos de Niquel Solidificados Rapidamente, M. Sc dissertation, Instituto de Pesquisas Energéticas e Nucleares, São Paulo, Brazil, 1992, p. 55.
17. Enami, K., Nenno, S. & Shimizu, *Trans JIM,* **14** (1973) 161.
18. Liu, C. T., White, C. L. & Horton, J. A., *Acta Metall.*, **33** (1985) 213
19. Lima, M. S. F. & Ferreira, P. I., submitted to *Scripta Metall. Mater.*